Dynamical Steady States in Driven Quantum Systems

T. M. Stace,[1,*] A. C. Doherty,[2] and D. J. Reilly[2]

[1]*ARC Centre for Engineered Quantum Systems, University of Queensland, Brisbane 4072, Australia*
[2]*ARC Centre of Excellence for Engineered Quantum Systems, School of Physics, The University of Sydney, Sydney, New South Wales 2006, Australia*

(Received 4 June 2013; published 30 October 2013)

We derive dynamical equations for a driven, dissipative quantum system in which the environment-induced relaxation rate is comparable to the Rabi frequency, avoiding assumptions on the frequency dependence of the environmental coupling. When the environmental coupling varies significantly on the scale of the Rabi frequency, secular or rotating wave approximations break down. We avoid these approximations, yielding dynamical steady states which account for the interaction between driven quantum dots and their phonon environment. The theory, which is motivated by recent experimental observations, qualitatively and quantitatively describes the transition from asymmetric unsaturated resonances at weak driving to population inversion at strong driving.

DOI: 10.1103/PhysRevLett.111.180602 PACS numbers: 05.60.Gg, 03.65.Yz, 42.50.Hz, 63.20.kd

Driven, dissipative quantum systems are ubiquitous in physics and chemistry, forming the basis for understanding the interaction of light and matter in phenomena ranging from solid-state quantum operations [1,2] to photosynthesis [3]. The basic physics of a dissipative, driven few-level system is understood via the Rabi or Jaynes-Cummings models for a driven two-level atom [4] coupled to a dissipative bosonic environment, leading to the optical Bloch equations [5]. Generically, the system response depends on the two-level energy splitting $\hbar\phi$, the Rabi frequency Ω, the environment-induced decay rate Γ, and the driving frequency ω_0. When $\phi \gg \Omega, \Gamma$, various approximations lead to *Markovian* descriptions of the dynamics, in which correlations between the system and its external environment are very short lived. Markovian models make distinct predictions, depending on the relative size of Γ and Ω. If $\phi \gg \Gamma \gg \Omega$, the weak driving produces small Lorentzian resonances in the system response, which are symmetric in the detuning $\tilde{\eta} = \phi - \omega_0$ [6–8]. If $\phi \gg \Omega \gg \Gamma$, the strong driving saturates the resonance, and excitation channels that are available when $\omega_0 > \phi$ lead to asymmetric resonances [1,9–11].

Experimentally, it is quite possible to enter a regime in which neither of these limits is valid. In particular, if Ω is large enough that the *spectral density* (which ultimately determines decay rates) varies substantially over a frequency range of bandwidth Ω, we can no longer assume a single decay rate and must account for coherences between different decay channels. Driven, semiconducting double-quantum-dot (DQD) devices, which are promising building blocks for a variety of new quantum technologies [12], can be driven very strongly [8,13], so they naturally fall into this category. In these devices, for which the electron-phonon coupling is significant [2,8,14–16], Γ or Ω may become large enough that Markovian approximations fail [17–19]. This is particularly important now that dynamical-decoupling techniques have managed to suppress decoherence from low-frequency noise (e.g., nuclear spins) [20], leaving residual electron-phonon coupling during fast quantum gate pulses as a potentially significant source of decoherence. Similar issues arise in superconducting [21,22] and photosynthetic systems [23,24], where the spectral density may vary substantially over a narrow bandwidth.

To address the limitations above, in this Letter, we derive a master equation that remains valid over the entire range of driving strengths, avoiding a number of conventional approximations. We first develop the general approach, which we then apply to the specific case of a DQD coupled to a phonon bath. Finally, we compute the response of the DQD to driving and discuss the qualitatively new features that emerge. These results replicate many of the phenomena observed in very recent experimental observations in a microwave-driven DQD [13].

We assume the Hamiltonian $H = H_S + H_I + H_B$ for the driven system, interaction, and harmonic bath, where $H_I = Z_S(\sum_{\mathbf{q}} g_{\mathbf{q}}^* a_{\mathbf{q}}^\dagger + \text{H.c.})$, Z_S is a system operator, $a_{\mathbf{q}}^\dagger$ is the bosonic bath creation operator for mode $\mathbf{q}$, and $g_{\mathbf{q}}$ is the system-bath coupling strength [5,11]. Since the system is driven, H_S has periodic time dependence. We transform to an interaction picture with respect to $H_0 = H_D + H_B$, where H_D acts trivially on the bath and has an associated set of Floquet eigenfrequencies $\mathcal{W}$ [25], giving $H(t) = H_S(t) + H_I(t)$, where $H_S(t) = \sum_{\omega\in\mathcal{W}} h_\omega e^{i\omega t}$,

$$H_I(t) = Z_S(t)\sum_{\mathbf{q}} g_{\mathbf{q}}^* a_{\mathbf{q}}^\dagger e^{i\omega_{\mathbf{q}} t} + \text{H.c.}, \tag{1}$$

$Z_S(t) = \sum_{\omega\in\mathcal{W}} P_\omega e^{i\omega t}$, and the Fourier coefficients h_ω and P_ω satisfy $h_{-\omega} = h_\omega^\dagger$ and $P_{-\omega} = P_\omega^\dagger$. We note that it is common to choose the dressing Hamiltonian $H_D = H_S$ so that $H_S(t) = 0$; however, we avoid this in order to later remove bath-induced dispersive shifts.

To derive the system dynamics, we iterate the von Neumann equation for the joint system-bath density matrix R, then trace over the bath [5]

$$\dot{\rho}(t) = -i[H_S(t), \rho(t)] - \mathrm{Tr}_B \int_0^t dt' \{H_I(t), [H_I(t'), R(t')]\},$$

where $\rho = \mathrm{Tr}_B R$ is the reduced system density matrix. Various approximations are often invoked to turn the integral into a convolution with a rapidly decaying kernel, yielding Markovian evolution [5]. Instead, we take a Laplace transform which we solve using an ansatz containing the relevant poles of the problem. Truncating the set of poles yields tractable approximations. The Laplace transform is (see the Supplemental Material [26])

$$\begin{aligned} s\bar{\rho}_s - \rho(0) = &-i \sum_{\omega' \in \mathcal{W}} [h_{\omega'}, \bar{\rho}_{s-i\omega'}] + \sum_{\omega', \omega'' \in \mathcal{W}} i(\tilde{J}(\omega' + is) \\ &- \tilde{J}(\omega'' - is)) P_{\omega'} \bar{\rho}_{s-i(\omega'-\omega'')} P^\dagger_{\omega''} \\ &- i\tilde{J}(\omega' + is) \bar{\rho}_{s-i(\omega'-\omega'')} P^\dagger_{\omega''} P_{\omega'} \\ &+ i\tilde{J}(\omega'' - is) P^\dagger_{\omega''} P_{\omega'} \bar{\rho}_{s-i(\omega'-\omega'')}, \end{aligned} \quad (2)$$

where $\bar{\rho}_s = \int_0^\infty dt' e^{-st'} \rho(t')$, $\tilde{J}(x) = \sum_q (|g_q|^2/\omega_q + x)$ is the generalized spectral density, and we assume that $R(t) \approx \rho(t) \otimes \rho_B$ for a thermal bath state ρ_B at zero temperature [26]. For later reference we define $\hat{J}$, J, and F as

$$\lim_{s \to 0^+} \pm i\tilde{J}(\omega \pm is) = \hat{J}_\pm(\omega) = (J(\omega) \pm iF(\omega))/2, \quad (3)$$

where $J(x) = 2\pi \sum_{\mathbf{q}} |g_{\mathbf{q}}|^2 \delta(\omega_{\mathbf{q}} + x)$ is the spectral density and $F(x) = -\pi^{-1} \int d\omega J(\omega)/(\omega - x)$ [5,27] (see the Supplemental Material [26]).

Since $\rho(t)$ is bounded, the Mittag-Leffler theorem implies that $\bar{\rho}_s$ is determined by its poles [28]. Suppose $\bar{\rho}_s$ has a pole at $s = z$; consistency between the right-hand and left-hand sides of Eq. (2) then requires additional poles in $\bar{\rho}_s$ at $s = z + i(\omega' - \omega'')$, where ω', $\omega'' \in \mathcal{W}$. This motivates the ansatz

$$\bar{\rho}_s = \sum_{\nu \in \mathcal{V}} \frac{\rho_\nu}{s - i\nu}, \quad (4)$$

where ρ_ν are as-yet-unknown residues. For consistency in Eq. (2), $\mathcal{V}$ is a countably infinite set, with $\mathcal{W} \subset \mathcal{V}$. To make progress, we truncate $\mathcal{V}$ to a finite set of the most significant poles and require that the residues of poles that appear on the left-hand side of Eq. (2) equal those on the right-hand side. This becomes exact in the limit that a complete set of poles is retained.

Since $\mathrm{Tr}\,\rho = 1$, ρ has a nonzero steady state, so $\bar{\rho}_s$ has a pole at $s = 0$. This suggests the simple but illuminating example in which we retain only this pole (i.e., $\mathcal{V} = \{0\}$), so $\bar{\rho}_s = \rho_0/s$, and the left-hand side of Eq. (2) becomes a constant (i.e., its residue is 0). The residue of the right-hand side at $s = 0$ should therefore vanish, yielding

$$0 = -i[h_0 - f_0, \rho_0] + \sum_{\omega \in \mathcal{W}} J(\omega) \mathcal{D}[P_\omega] \rho_0, \quad (5)$$

where $f_0 = \sum_\omega F(\omega) P^\dagger_\omega P_\omega/2$ and $\mathcal{D}[A]\rho \equiv A\rho A^\dagger - (A^\dagger A \rho + \rho A^\dagger A)/2$ is the Lindblad superoperator. The solution to Eq. (5) is the steady state of the conventional Markovian dynamics [5,11]. Furthermore, F yields a dispersive Lamb shift that renormalizes the system dynamics. Choosing H_D such that $h_0 = f_0$ cancels the dispersive effects arising from the bath, so that the *renormalized* system Hamiltonian vanishes in this interaction picture.

In general, consistency between residues appearing on the left-hand and right-hand sides of Eq. (2) as $s \to i\nu'$ requires

$$\begin{aligned} i\nu' \rho_{\nu'} = &-i \sum_{\nu \in \mathcal{V}} [h_{\nu'-\nu}, \rho_\nu] + \sum_{\substack{\nu \in \mathcal{V}, \omega \in \mathcal{W}, \\ \omega' = \omega + \nu - \nu'}} \{(\hat{J}_+(\omega - \nu') \\ &+ \hat{J}_-(\omega + \nu)) P_\omega \rho_\nu P^\dagger_{\omega'} - (\hat{J}_+(\omega \\ &- \nu') \rho_\nu P^\dagger_{\omega'} P_\omega + \hat{J}_-(\omega + \nu) P^\dagger_{\omega'} P_\omega \rho_\nu)\}. \end{aligned} \quad (6)$$

The residues appearing in Eq. (4) are bounded matrices, so we see from Eq. (6) that $\|\rho_{\nu'}\| \sim |\hat{J}/\nu'|$; i.e., the size of the residue decreases with the magnitude of the pole. As above, we choose H_D so that $h_\omega = f_\omega$ to cancel dispersive terms in Eq. (6). This choice fixes the poles that appear in $\mathcal{W}$. The $\hat{J}$-dependent terms arising on the right-hand side of Eq. (6) can be written as a sum of (a) dissipative J-dependent terms, analogous to the Lindblad terms in Eq. (5), (b) dispersive terms of the form $i[f_{\nu'-\nu}, \rho_\nu]$, where f_ν depends on F, which are eliminated by the correct choice of H_D analogous to f_0 in Eq. (5), and (c) residual inhomogeneous F-dependent terms, which cannot be eliminated.

To compute the transient dynamics of a system, we should retain poles with negative real values. In what follows, we will be concerned with steady-state properties of a system operator $M(t) = \sum_{\omega \in \mathcal{W}} M_\omega e^{i\omega t}$, and so we consider only pure-imaginary poles. The Laplace transform is $\bar{M}_s = \sum_{\omega \in \mathcal{W}} \mathrm{Tr}\{M_\omega \bar{\rho}_{s-i\omega}\}$, and the time-averaged, steady-state expectation is the residue of $\bar{M}_s$ at $s = 0$, i.e., $\langle M \rangle_0 \equiv \overline{\mathrm{Tr}\{M(t)\rho(t)\}} = \sum_{\nu \in \mathcal{V}} \mathrm{Tr}\{M^\dagger_\nu \rho_\nu\}$. Importantly, this depends on both the time-averaged steady state ρ_0 and the dynamical residues $\rho_{\nu \neq 0}$.

We note that the dynamical poles in the ansatz yield non-Markovian evolution: in the dressed basis, Markovian dynamics leads to stationary steady states, which implies $\rho_{\nu \neq 0} = 0$. This corresponds to the simplest approximation $\mathcal{V} = \{0\}$ discussed above.

Using this formalism, we now turn to the example of a microwave-driven, one-electron DQD system with localized left $|l\rangle$, or right $|r\rangle$, states separated by a distance d, interdot bias ϵ, and interdot tunneling rate Δ, driven at frequency ω_0 and amplitude Ω_0, coupled to a phonon bath [6,11,29]. The driven system Hamiltonian is

$$H_S = -(\epsilon\sigma_z + \Delta\sigma_x)/2 + \Omega_0\cos(\omega_0 t)(\cos\delta\sigma_z + \sin\delta\sigma_x),$$
$$= -\phi\sigma_z^e/2 + \Omega_0\cos(\omega_0 t)(\cos(\theta-\delta)\sigma_z^e - \sin(\theta-\delta)\sigma_x^e),$$

where $\sigma_z \equiv |l\rangle\langle l| - |r\rangle\langle r|$ and $\sigma_x \equiv |l\rangle\langle r| + |r\rangle\langle l|$. The qubit splitting is $\phi = (\epsilon^2 + \Delta^2)^{1/2}$ in the energy eigenbasis $\{|g\rangle, |e\rangle\}$, $\sigma_z^e = \sin\theta\sigma_x + \cos\theta\sigma_z$, $\sigma_x^e = \cos\theta\sigma_x - \sin\theta\sigma_z$, and $\theta = \arctan(\Delta/\epsilon)$. In a frame rotating at the driving frequency ω_0 (and dropping terms with frequency $\pm 2\omega_0$ [30]), H_S becomes time independent

$$H_S = -(\tilde{\eta}\sigma_z^e + \tilde{\Omega}\sigma_x^e)/2 \equiv -\tilde{\Omega}'(\cos\tilde{\varphi}\sigma_z^e + \sin\tilde{\varphi}\sigma_x^e)/2, \tag{7}$$

where $\tilde{\eta} = \phi - \omega_0$, $\tilde{\Omega} = \Omega_0\sin(\theta-\delta)$, $\tilde{\varphi} = \arctan(\tilde{\Omega}/\tilde{\eta})$, and $\tilde{\Omega}' = (\tilde{\Omega}^2 + \tilde{\eta}^2)^{1/2}$ (here, the tildes denote bare quantities).

We transform to an interaction picture defined by

$$H_D = -(\eta\sigma_z^e + \Omega\sigma_x^e)/2 = -\Omega'\sigma_z^d/2,$$

in the dressed basis $\{|-\rangle, |+\rangle\}$, $\sigma_z^d = \cos\varphi\sigma_z^e + \sin\varphi\sigma_x^e$, $\varphi = \arctan(\Omega/\eta)$, and $\Omega' = (\Omega^2 + \eta^2)^{1/2}$. This gives the Fourier coefficients of $H_S(t)$ defined earlier: $h_0 = -[\tilde{\Omega}'\cos(\tilde{\varphi} - \varphi) - \Omega']\sigma_z^d/2$ and $h_{\pm\Omega'} = -\tilde{\Omega}'\sin(\tilde{\varphi} - \varphi)\sigma_\pm^d/2$. We emphasize that η and Ω in H_D will be chosen below to cancel bath-induced dispersive terms.

The electron-phonon coupling Hamiltonian is given by Eq. (1) with $Z_S = \sigma_z$ [11,31,32]. $Z_S(t)$ has Fourier frequencies $\mathcal{W} = \pm\{0, \Omega', \omega_0, \omega_0 \pm \Omega'\}$ and coefficients $P_0 = \alpha_0\sigma_z^d$, $P_{\Omega'} = \alpha_{\Omega'}\sigma_+^d$, $P_{\omega_0\pm\Omega'} = \alpha_{\omega_0\pm\Omega'}\sigma_\pm^d$, and $P_{\omega_0} = \alpha_{\omega_0}\sigma_z^d$, where $\alpha_0 = \cos\theta\cos\varphi$, $\alpha_{\Omega'} = -\cos\theta\sin\varphi$, $\alpha_{\omega_0\pm\Omega'} = \mp\sin\theta(1 \pm \cos\varphi)/2$, and $\alpha_{\omega_0} = -\sin\theta\sin\varphi/2$ [11].

To illustrate the significance of the dynamical poles, we choose $\mathcal{V} = \{0, \pm\Omega'\}$. Note that Ω' is the *renormalized* Rabi frequency, which is fixed once H_D is chosen to eliminate dispersive shifts. The dispersive terms appearing in Eq. (6) are $f_0 = a_0\sigma_z^d/2$ and $f_{\pm\Omega'} = a_{\Omega'}\sigma_\pm^d/2$, where

$$a_0 = (-\alpha^2_{\omega_0-\Omega'}F_{\omega_0-\Omega'} + \alpha^2_{\omega_0+\Omega'}F_{\omega_0+\Omega'} + \alpha^2_{\Omega'}F_{\Omega'})/2,$$
$$a_{\Omega'} = \alpha_{\omega_0}(\alpha_{\omega_0-\Omega'}F_{\omega_0-\Omega'} - \alpha_{\omega_0+\Omega'}F_{\omega_0+\Omega'}) - \alpha_0\alpha_{\Omega'}F_{\Omega'}, \tag{8}$$

and $F_x \equiv F(x) - F(-x)$. Setting $h_\nu = f_\nu$ to cancel dispersive terms yields the required relationship between the bare $\tilde{\eta}$ and $\tilde{\Omega}$ and the renormalized η and Ω

$$\begin{bmatrix}\tilde{\eta}\\ \tilde{\Omega}\end{bmatrix} = -\begin{bmatrix}\cos\varphi & -\sin\varphi\\ \sin\varphi & \cos\varphi\end{bmatrix}\begin{bmatrix}a_0 - \Omega'\\ a_{\Omega'}\end{bmatrix}. \tag{9}$$

We solve this nonlinear equation numerically for η and Ω.

The renormalization of the detuning arises from the phonon-induced Lamb shift [5]. This shift depends on the phonon modes with which the driven system is most strongly coupled, which depends itself on detuning [11], resulting in a detuning-dependent Lamb shift. The renormalization of the Rabi frequency is related to the polaron transformation [10,33], in which pure-electronic modes are renormalized to polaronic modes with larger effective mass, reducing the transition dipole moments.

Differences between the bare and renormalized quantities ultimately depend on the electron-phonon coupling via F, which appears in a_0 and $a_{\Omega'}$. Very close to resonance $\tilde{\eta} \approx 0$, some intuition into the effect of the dispersive shifts can be gained by expanding the right-hand side of Eq. (9) in powers of Ω' and then solving to find

$$\eta_{\text{approx}} \approx \tilde{\eta}/(1 + F'(0)) + O[\tilde{\eta}^3/\tilde{\Omega}^2], \tag{10a}$$
$$\Omega_{\text{approx}} \approx \tilde{\Omega}/(1 - F'(0)) + O[\tilde{\eta}^2/\tilde{\Omega}]. \tag{10b}$$

Thus, the renormalized detuning and Rabi frequency are scaled with respect to the bare values. Importantly, the scaling factors depend (nonperturbatively) on $F'(0)$.

Focusing on the specific case of bulk piezoelectric phonon coupling, the spectral density is [11]

$$J(\omega^*) = \begin{cases}\pi\mathsf{P}|\omega^*|\frac{1-\mathrm{sinc}(d^*\omega^*)}{1+(\omega^*/\omega_c^*)^2} & \text{if } \omega^* < 0\\ 0 & \text{if } \omega^* \geq 0,\end{cases} \tag{11}$$

where $\omega^* \equiv \omega/\omega_0$, $d^* \equiv d\omega_0/c_s$, and P are, respectively, nondimensionalized frequency, interdot separation, and coupling strength (c_s is the speed of sound) [27]. The high-energy cutoff ω_c^* is determined by the spatial extent of the localized wave functions $|l\rangle$, $|r\rangle$. Figure 1 shows J and F [which also has an analytic expression (see the Supplemental Material [26])]. The interdot separation results in double-slit-like interference as phonons interact with the localized states, causing oscillations in J and F, with a spectral period $\approx 2\pi/d^*$ [1,11]. This leads to a low-frequency cutoff $\sim 1/d^*$ in J. Between the low- and high-frequency cutoffs, J is Ohmic with a superimposed oscillatory modulation.

$F'(0)$ determines the renormalization strength. We can calculate $F'(0)$ exactly (see the Supplemental Material [26]), but a good estimate is obtained by noting that $F'(0) = -\pi^{-1}\int d\omega J(\omega)/\omega^2$. Combined with the facts that

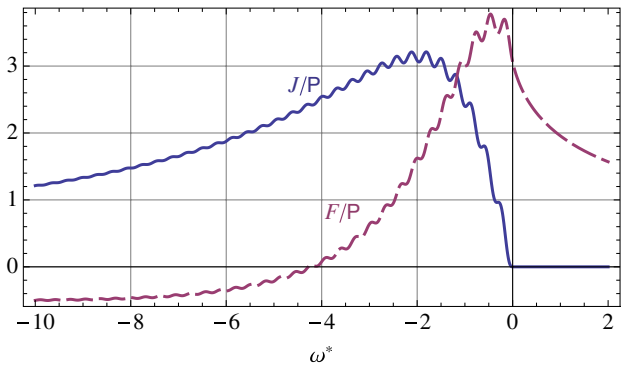

FIG. 1 (color online). Dependence of J (solid line) and F (dashed line) on ω, for $\omega_c^* = 2$ and $d^* = 20$.

$J \approx \pi \mathsf{P}|\omega|$ for $\omega \in [-\omega_c^*, -1/d^*]$ and it decays rapidly outside this interval, we find that $F'(0) \approx -\mathsf{P}\log(d^*\omega_c^*) < 0$. Thus, the high- and low-frequency cutoffs appear as a ratio in the renormalization strength. It follows from Eq. (10) that near resonance, the renormalized detuning is larger than the bare value, while the renormalized Rabi frequency is smaller.

Figure 2 shows the effects of renormalization on η and Ω. The renormalized quantities (solid curves) are modified most strongly close to resonance. Near resonance, the renormalized detuning is steeper than the bare detuning (dashed curve), consistent with the argument above. The renormalized Rabi frequency (bottom panel, solid curve) is lower than the bare value (dashed curve) and is well approximated by Eq. (10b) near resonance.

The theoretical framework discussed here differs from Markovian models in two respects: it includes contributions arising from (a) the dynamical steady state of the driven system and (b) the bath-induced renormalization of the system in which H_D is chosen self-consistently to remove dispersive shifts and define the poles in $\mathcal{W}$. We elucidate these contributions by manually suppressing each effect and comparing with the fully dynamical, renormalized result. We illustrate this by calculating the right dot population $M = |r\rangle\langle r| = (1 - \sigma_z)/2$ [6], which models an electrometer adjacent to the DQD [8,34].

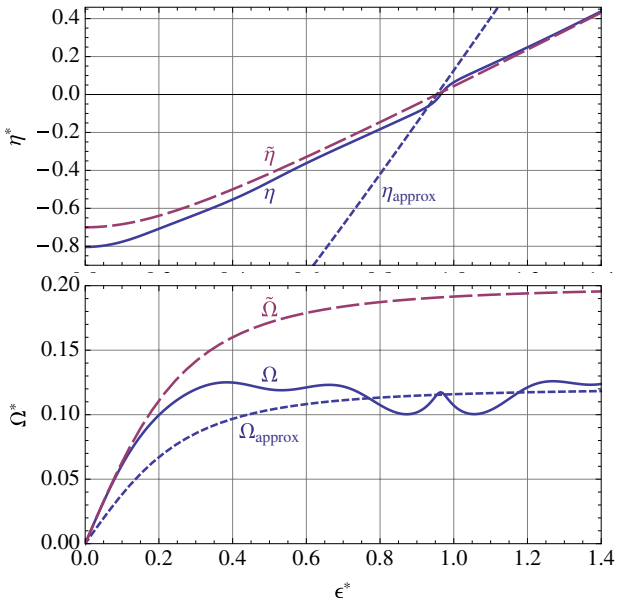

FIG. 2 (color online). Top: detuning versus bias. Bottom: Rabi frequency versus bias. Dashed curves: bare detuning $\tilde{\eta}$ and Rabi frequency $\tilde{\Omega}$. Solid curves: renormalized detuning η and Rabi frequency Ω obtained by solving Eq. (9). Dotted curves: near-resonance approximations to renormalized quantities from Eq. (10); η_{approx} captures the steeper slope of η close to resonance. Parameters are $\Delta^* = 0.3$, $\delta = \pi/2$, $\omega_c^* = 2$, $d^* = 20$, $\Omega_0^* = 0.2$, and $\mathsf{P} = 0.2$. Resonance occurs at $\epsilon^* = (1 - \Delta^{*2})^{1/2} \approx 0.954$.

Figure 3 shows the time-averaged, steady-state population $\langle M\rangle_0$ for relatively weak driving (top) and relatively strong driving (bottom). The solid curves show the dynamical, renormalized results; the dashed curve retains the dynamical poles but neglects renormalization [35]; and the dotted curve neglects both, corresponding to the strong-driving Markov approximation [11]. The resonant peaks exhibit strong phonon-induced asymmetry, which becomes more pronounced at higher driving, to the extent of exhibiting population inversion on the blue-detuned side [9,11]. The enhancement of the blue-detuned wing is a consequence of photon absorption from the driving field accompanied by a Raman phonon emission, leading to a higher rate of excitation compared to the relaxation rate [11]. At weak driving, the resonant peak is unsaturated ($\langle M\rangle_0 < 0.5$) [Fig. 3 (top)], but this is only evident when dynamical poles are included (solid and dashed curves); suppressing dynamical poles necessarily yields a saturated peak on resonance, i.e., $\langle M\rangle_0 = 0.5$ at $\eta = 0$ (dotted curves). Consistent with Fig. 2, the effects of parameter renormalization are most significant near resonance, narrowing the central resonant peak. This occurs for two reasons: as ϵ moves away from resonance, the renormalized detuning changes more rapidly with ϵ than does the bare detuning, and the renormalized Rabi frequency decreases below its resonant value.

Following Eq. (6) we noted that there are residual F-dependent terms in Eq. (6) that cannot be canceled. This is manifested as subtle "shoulders" appearing on the red-detuned side of the resonance ($\phi > \omega_0$), as shown in the inset to Fig. 3 (bottom), resulting in non-Lorentzian decay

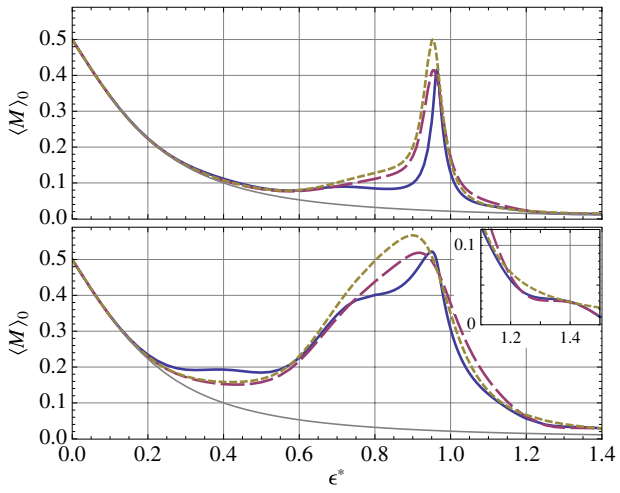

FIG. 3 (color online). Top: time-averaged steady-state population of the right dot $\langle M\rangle_0 = \langle |r\rangle\langle r|\rangle_0$ for relatively weak driving $\Omega_0^* = 0.07$. Bottom: $\langle M\rangle_0$ for stronger driving $\Omega_0^* = 0.2$. Inset: zoom-in of red-detuned wing. Different curves correspond to different levels of approximation. Solid dark curve: $\mathcal{V} = \{0, \pm\Omega'\}$ and renormalized η, Ω. Dashed curve: $\mathcal{V} = \{0, \pm\Omega'\}$ and bare $\tilde{\eta}$, Ω_{approx}. Dotted curve: $\mathcal{V} = \{0\}$ and bare $\tilde{\eta}$, Ω_{approx}. Solid light curve: no driving. Other parameters are as in Fig. 2.

of the red-detuned wings. In this regime, the microwave photons have insufficient energy to drive real transitions between the energy eigenstates, highlighting the fact that the shoulders are a consequence of dispersive, rather than dissipative, electron-phonon coupling.

Phenomena such as the transition from asymmetric unsaturated resonances at weak driving to population inversion at strong driving, and phonon-induced shoulders have been observed experimentally [13]. Our theory yields good qualitative agreement and reasonable quantitative agreement with these experimental results. Intriguing connections exist between our approach and a non-Markovian extension to Redfield theory [18,23].

In conclusion, we have derived a set of coupled equations for the residues of dynamical poles of the reduced density matrix of a system. These terms yield steady-state dynamics which are absent from Markovian treatments, as well as nonperturbative renormalization of the bare system parameters. Neglecting either the dynamical poles or the effects of renormalization yields qualitatively different results, particularly near resonance. The theory is consistent with recent experimental results which exhibit the same bath-induced phenomena discussed here. Our formalism permits arbitrarily many Floquet eigenfrequencies in the driven Hamiltonian and so extends straightforwardly to higher harmonics.

This research was supported by the Office of the Director of National Intelligence, Intelligence Advanced Research Projects Activity (IARPA), through the Army Research Office Grant No. W911NF-12-1-0354, and by the Australian Research Council via the Centre of Excellence in Engineered Quantum Systems (EQuS), Project No. CE110001013. We thank S. Barrett, J. Colless, J. Coombes, X. Croote, G. Milburn, A. Nazir, and A. Shabani for illuminating discussions.

*stace@physics.uq.edu.au

[1] P. Roulleau, S. Baer, T. Choi, F. Molitor, J. Güttinger, T. Müller, S. Dröscher, K. Ensslin, and T. Ihn, Nat. Commun. **2**, 239 (2011).
[2] G. Granger, D. Taubert, C. E. Young, L. Gaudreau, A. Kam, S. A. Studenikin, P. Zawadzki, D. Harbusch, D. Schuh, W. Wegscheider *et al.*, Nat. Phys. **8**, 522 (2012).
[3] A. Ishizaki and G. R. Fleming, Proc. Natl. Acad. Sci. U.S.A. **106**, 17 255 (2009).
[4] D. Braak, Phys. Rev. Lett. **107**, 100401 (2011).
[5] C. W. Gardiner and P. Zoller, *Quantum Noise* (Springer, New York, 2000).
[6] S. D. Barrett and T. M. Stace, Phys. Rev. Lett. **96**, 017405 (2006).
[7] T. M. Stace and S. D. Barrett, Phys. Rev. Lett. **92**, 136802 (2004).
[8] J. R. Petta, A. C. Johnson, C. M. Marcus, M. P. Hanson, and A. C. Gossard, Phys. Rev. Lett. **93**, 186802 (2004).
[9] M. I. Dykman, Sov. J. Low Temp. Phys. **5**, 89 (1979).
[10] T. Brandes and B. Kramer, Phys. Rev. Lett. **83**, 3021 (1999).
[11] T. M. Stace, A. C. Doherty, and S. D. Barrett, Phys. Rev. Lett. **95**, 106801 (2005).
[12] R. Hanson, L. P. Kouwenhoven, J. R. Petta, S. Tarucha, and L. Vandersypen, Rev. Mod. Phys. **79**, 1217 (2007).
[13] J. I. Colless, X. G. Croot, T. M. Stace, A. C. Doherty, S. D. Barrett, H. Lu, A. C. Gossard, and D. J. Reilly, arXiv:1305.5982.
[14] T. Hayashi, T. Fujisawa, H. D. Cheong, Y. H. Jeong, and Y. Hirayama, Phys. Rev. Lett. **91**, 226804 (2003).
[15] T. H. Oosterkamp, T. Fujisawa, W. G. van der Wiel, K. Ishibashi, R. V. Hijman, S. Tarucha, and L. P. Kouwenhoven, Nature (London) **395**, 873 (1998).
[16] T. Fujisawa, T. H. Oosterkamp, H. Tjerk, W. G. van der Wiel, B. W. Broer, R. Aguado, S. Tarucha, and L. Kouwenhoven, Science **282**, 932 (1998).
[17] C. Weber, A. Fuhrer, C. Fasth, G. Lindwall, L. Samuelson, and A. Wacker, Phys. Rev. Lett. **104**, 036801 (2010).
[18] A. Ishizaki and Y. Tanimura, J. Phys. Soc. Jpn. **74**, 3131 (2005).
[19] D. McCutcheon and A. Nazir, New J. Phys. **12**, 113042 (2010).
[20] M. J. Biercuk and D. J. Reilly, Nat. Nanotechnol. **6**, 9 (2010).
[21] C. M. Wilson, G. Johansson, T. Duty, F. Persson, M. Sandberg, and P. Delsing, Phys. Rev. B **81**, 024520 (2010).
[22] S. Gasparinetti, P. Solinas, S. Pugnetti, R. Fazio, and J. P. Pekola, Phys. Rev. Lett. **110**, 150403 (2013).
[23] A. Ishizaki and Y. Tanimura, Chem. Phys. **347**, 185 (2008).
[24] A. K. Ringsmuth, G. J. Milburn, and T. M. Stace, Nat. Phys. **8**, 562 (2012).
[25] M. M. Maricq, Phys. Rev. B **25**, 6622 (1982).
[26] See the Supplemental Material http://link.aps.org/supplemental/10.1103/PhysRevLett.111.180602 for details. It is straightforward to include finite temperatures in the formalism.
[27] This form of the spectral density reverses the common convention for which $J(\omega) = 0$ for $\omega < 0$.
[28] H. Jeffreys and B. Jeffreys, *Methods of Mathematical Physics* (Cambridge University Press, Cambridge, England, 1999).
[29] T. M. Stace, S. D. Barrett, H.-S. Goan, and G. J. Milburn, Phys. Rev. B **70**, 205342 (2004).
[30] This is not critical to the approach and can be corrected by including more Floquet terms [4,25].
[31] G. D. Mahan, *Many-Particle Physics* (Plenum, New York, 1981).
[32] S. Rahman, T. M. Stace, H. P. Langtangen, M. Kataoka, and C. H. W. Barnes, Phys. Rev. B **75**, 205303 (2007).
[33] D. P. S. McCutcheon and A. Nazir, Phys. Rev. Lett. **110**, 217401 (2013).
[34] D. J. Reilly, C. M. Marcus, M. P. Hanson, and A. C. Gossard, Appl. Phys. Lett. **91**, 162101 (2007).
[35] We use the rescaled Rabi frequency Ω_{approx} so that the effective driving amplitude is comparable near resonance.